Large Size Heat Pumps Advanced Cost Functions Introducing the Impact of Design COP on Capital Costs

Authors: Alberto Vannoni[1], Alessandro Sorce*[1], Alberto Traverso[1], Aristide Fausto Massardo[1]

[1] University of Genoa, Thermochemical Power Group, Via Montallegro 1, 16145 Genoa, Italy

* Corresponding author: Alessandro Sorce (alessandro.sorce@unige.it)

Highlights:

- The impact on capital costs of COP, fluid, and operating temperatures is quantified
- Dependency of capital cost on COP can be described by a power function
- The best fluid differs if thermodynamic or economic optimum is pursued
- Cost functions derived by a multi-objective optimization are provided for fast replication

Keywords: Heat pump, Thermo-economics, Multi-objective Optimization, Cost functions

Abstract:

Power-to-heat technologies are today promising solutions supplying low-carbon heat and coupling the electricity and heating sectors. Moreover, the development of high-temperature heat pumps enables the provision of process heat, as in the food industry and early generation district heating networks. However, high capital cost often jeopardizes their viability. Fluid selection is a key design parameter affecting both variable and capital (TCI) costs since the thermodynamic features impact both the Coefficient of Performance, COP, and equipment sizing. As a consequence, identifying the best fluid and estimating the capital cost by employing simple and reliable cost functions is essential to assess opportunities for heat pumps in the market. By means of a techno-economic model and a multi-objective optimization strategy, this paper provides a new method to identify the best heat pump solution considering different source and supply temperatures. The proposed Pareto analysis is used to fit new and updated cost functions for heat pumps considering the working fluid, the source and supply temperatures, and the impact of design COP on TCI. The resulting methodology is expected to facilitate the uptake of heat pumps for electrification of the industrial sector, especially for high temperature applications potentially displacing the use of natural gas boilers.

1. Introduction

One of the most challenging targets toward a net-zero carbon economy is the research for feasible solutions to cut the emissions related to thermal demand. Heat is currently supplied mainly by the direct combustion of fossil fuels, 64% in 2021 worldwide, mainly natural gas [1]. However, Heat pumps (HPs), modern biofuel combustion, thermal solar, and geothermal are today increasing their relevance and are promising solutions to improve the sustainability of heating. Furthermore, HPs link the electricity and heating sectors, paving the way to future synergy with potential mutual benefits [2].

Nevertheless, solar thermal and geothermal rely on the availability of the source, thus they are suitable to cover only a fraction of the overall demand, while HPs can be operated steadily and can become particularly attractive wherever there is a good thermal source to exploit. For example, HPs may effectively recover high-temperature waste heat from industrial processes, electricity generation, or, at a lower temperature, from data centers and metro systems [3–6]. HPs are commercially available for supplying heat up to 80-100°C, but as the temperature increases the technology readiness level decreases [7]. Together with the need of adopting environmentally friendly fluids and limiting capital expenditures, the increase in achievable temperature of supply is the main challenge for an effective design of vapor compression HP.

A key aspect of the design of HPs is the selection of working fluid which is governed by multiple factors. Thermodynamic characteristics of the fluid impose limits concerning the source and supply temperature and the best achievable COP: for instance, operating close to the fluid critical temperature causes condensing latent heat to decrease dramatically, thus affecting HPs performance. Moreover, fluid characteristics affect heat exchange effectiveness, thus the exchangers sizing and cost. Thermodynamic properties also influence the Volumetric Heat Capacity (VHC) (i.e., the heat capacity per unit of volumetric flow), which is also directly reflected in the size and cost of HP's components, such as the compressor. Eventually, fluid selection impacts compressor discharge temperature and pressure. High pressures should be avoided for practical and cost-effective design: in this paper, a limit of 50 bar is imposed. Similarly, if the compressor requires lubrification, high discharge temperature must be avoided since it causes oil degradation, and thus, it is desirable to keep it below 135°C to ensure an adequate life. At temperatures higher than 150°C, oil degradation is possible, and, in the presence of oxygen, ignition is a risk as well. However, using mineral oil or a synthetic polyglycol lubricant, it is possible to extend the temperature limit, which under no circumstances should exceed 180°C, a common limit for standard HPs design [8,9].

Fluid selection is also a matter of environmental impact: potentially ozone-depletive fluids (CFCs and HCFCs) are no longer considered for the design of new HPs. Furthermore, the Doha amendment to the Kyoto Protocol [10] imposes a progressive phase-out of fluids presenting a Global Warming Potential (GWP) higher than 1000. Consequently, alternatives to HFCs industry standards for low-medium temperatures and HTHP applications, such as R134a and R245fa respectively, are needed. The interest for a fourth generation of fluids is mainly in natural fluids (e.g., ammonia, water, CO_2, or hydrocarbons) or Hydrofluoroolefins (HFOs).

Regarding natural fluids, they are appreciated for their availability. In particular, Ammonia (R717) is already widely used [11], for its increased VHC with respect to other fluids [12] and high performance obtainable for chilling units. Nevertheless, it implies relevant operating pressure, and its toxicity and flammability must be considered when designing an HP with a relevant charge of fluid. Moreover, when ammonia is released into the atmosphere reacts with several compounds and produces aerosols and hence increasing the concentrations of particulate air pollutants (PM2.5) [13]. However, even if all the existing HPs operating with CFCs, HCFCs, or HFCs were to be replaced by ammonia HPs, ammonia emitted by such HPs would be negligible compared to that from agriculture or industrial and residential activities [14]. Water (R718) is interesting for applications beyond 150°C supply temperature, but high vapor's specific volume and required considerable pressure ratios hinder its application [15,16]. Transcritical CO_2 (R744) cycles are promising, however, they require a dedicated design because of the supercritical state of the fluid in many components and of the high operating pressure (critical pressure 73.6 bar), thus are not investigated in this paper. Among hydrocarbons, iso-butane (R600a), butane (R600), and pentane (R601) are the most promising fluids for HTHPs because of their high critical temperatures at reasonable pressures (134.7°C, 152.0°C, and 196.6°C at 36.3, 38.0, and 33.7 bar, respectively); for lower temperatures, propane (R290) is a good candidate for replacement of R134a [17], or R22 if mixed with ethane R170 [18]. The criticism about hydrocarbons arises because of their flammability since all of them are classified as highly flammable (A3) by ASHRAE [19].

Hydrofluoroolefins, HFOs, are more complex molecules, inevitably more expensive to synthesize [20]. HFOs are considered environmentally friendly because of their almost zero GWP, but once released into the atmosphere, they quickly degrade to Trifluoracetic acid (TFA), which is potentially harmful to the environment and the biosphere [21]. However, a recent review points out the numerous gaps in knowledge and the impossibility to draw any conclusion about the real contribution of anthropogenic TFA with respect to the natural [22]. Moreover, the Assessment Report of the UN Ozone Secretariat [14] remarks that there is no evidence that these local depositions of TFA will result in risks to the environment, especially when eventual dilution occurs in oceans. Among the possible HFOs candidates for HTHPs, R1336mmz(Z) and R1234ze(Z) are appreciated for their zero

ODP, low GWP, and flammability [23], while R1234yf and R1234ze(E) are attractive replacements for R134a for lower temperature applications. Finally, some hydrochlorofluoroolefins (HCFOs), distinguished from HFOs by the presence of chlorine and thus having non-zero, even low (~10^{-4}), ODP [23,24], show an interesting potential for HTHP, like R1233zd(E) or R1224yd(Z) [25].

Finally mixing different fluids within azeotropic or non-azeotropic mixtures is currently an open research topic significantly increasing the possibility of optimizing environmental and techno-economic indicators [26,27].

Many authors [25,28–32] have reviewed and compared the possible fluids and cycles for HTHP applications focusing on the fluid physical properties or cycle thermodynamic potentialities, nevertheless, any economic consideration is limited, if included, to the VHC estimation. Therefore, currently, a lack of knowledge about the techno-economic performance and the viability of high-temperature HPs exists. T. Ommen et al. [33] quantify the cost of HPs operating with R134a, R290, R600a, R717, and R744 imposing a 5 K temperature difference at evaporator and condenser pinch point in all circumstances. Similarly, this paper introduces, within the following section, a model for both cycle performance, related to operational expenditure and capital expenditure assessment of heat pumps. Furthermore, through a multi-objective optimization, it explores the impact of increased COP on capital costs systematically optimizing the heat exchangers design and superheating of vapor at the compressor suction. This approach allows for identifying the Pareto fronts, i.e., the sets of nondominated solutions whose objectives (COP and TCI) cannot be improved except to the detriment of each other. The analysis focuses on low-GWP fluids, considering different sources and sinks, and comparing them with consolidated standard fluids. The third section concludes the described analysis by proposing the best fluid for each possible application (i.e., each combination of supply and source temperature). Subsequently, in Section 4, by regressing the Pareto fronts, new “optimal” cost functions are provided considering the possibility of pursuing either a thermodynamic or cost optimization, allowing a proper balance of operational and capital cost: this represents a novel step further in the HPs thermoeconomic optimization approach to the authors’ best knowledge. Finally, Section 5 considers three case studies applying the proposed cost function to assess the replacement of a gas-fired boiler to supply heat at three different thermal levels.

2. Methodology

2.1. Techno-economic detailed model

In order to carry out the analysis reported in this paper, a new and updated techno-economic model heat pump performance was developed on the basis of the WTEMP EVO software approach, proprietary to the University of Genoa, allowing for thermoeconomic analysis and optimization of innovative energy systems at on-design conditions, considering the real-gas properties [34,35]. The model works through two subsequent steps. Within the first step, the cycle is designed to seek the maximum COP, i.e., the minimum condensing pressure and maximum evaporating pressure. In the second step, each component is sized and the relative Purchased Equipment Cost (PEC) is estimated. According to the approach proposed by Bejan [36], the Total Investment Cost (TCI) is assessed by multiplying by a factor of 4.16 the sum of all PECs, therefore accounting also for installation, piping, instrumentation, electrical equipment engineering, supervision, as well as start-up and working capital (e.g., working fluid).

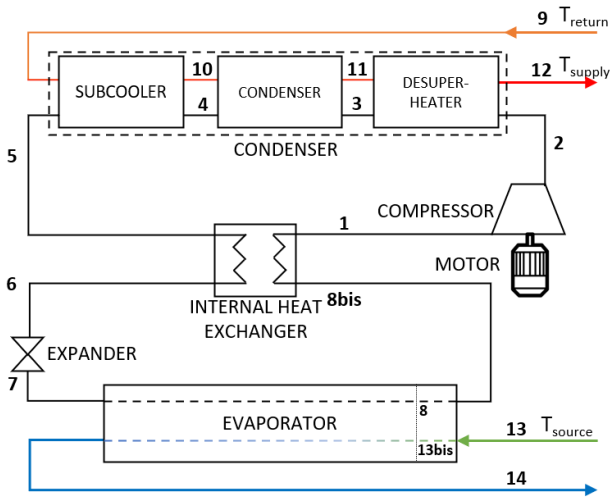

Figure 1: Reference vapor compression heat pump layout

The reference vapor compression cycle includes a single-stage compressor and an Internal Heat Exchanger (Figure 1). Such a cycle is defined by assuming the following input variables:

- HP capacity (Q_{COND}), thermal power delivered to the sink from the condenser
- Supply temperature (T_{12}), the temperature at which the heat transfer fluid, commonly water, is heated up
- Source temperature (T_{13}), the temperature at which the heat source is available
- Temperature difference at the sink (ΔT_{sink}= T_{12} -T_9), the return heat transfer fluid temperature, commonly it is correlated to the supply temperature
- Temperature difference for the source fluid (ΔT_{source}= T_{13}-T_{14}), this parameter describes the source heat abundancy
- Working fluid
- Compressor isentropic efficiency
- Minimum pinch point temperature differences at each heat exchanger (ΔT_{HXpp_min})
- Required superheating at the compressor suction (ΔT_{SH})
- Fraction of superheating provided by the evaporator, χ, as defined by equation (1), where 8 represents the saturated vapor status, occurring inside the evaporator

$$\chi = \frac{T_{8bis} - T_8}{T_1 - T_8} \cdot 100 = \frac{\Delta T_{SHbis}}{\Delta T_{SH}} \cdot 100 \quad (1)$$

Regarding the first calculation step, the model, developed in MATLAB, solves the cycle iteratively, solving heat and mass balances on the components at on-design conditions: further information can be found in previous works [37]. Reciprocating pistons compressor volumetric efficiency is assessed according to the pressure ratio considering a swept volume of 1%, its isentropic efficiency is assumed 80% [33], and electric motor efficiency is 95%.

Concerning the difference between the supply and the return temperature (ΔT_{sink}) the following rule of thumb was deduced from literature data for DHN applications [38]:

$$\Delta T_{sink} = 10 + \frac{T_{supply}\ [°C]}{3} \quad (2)$$

Regarding the second calculation step, once thermodynamic on-design conditions are defined, the model addresses the TCI and KPIs evaluation. First, the WTEMP EVO-based model sizes each component. For heat exchangers the logarithmic mean temperature difference method is adopted, assuming counter-flow arrangement: in the following equations (3) and (4) the labels “1” and “2” refer to the two sides of the heat exchanger.

$$A = \frac{\dot{Q}}{U \cdot LMTD} \tag{3}$$

$$LMTD = \frac{\Delta T_1 - \Delta T_2}{\ln\left(\frac{\Delta T_1}{\Delta T_2}\right)} \tag{4}$$

As it is possible to appreciate from equation (3), to assess the heat exchanger area, that is the cost function input variable, a proper estimation of heat transfer coefficient U is pivotal, and it depends on the flow characteristics and heat exchanger geometry.

For the purpose of this paper, a simplified approach to assess U is proposed. The overall heat transfer coefficient is the reciprocal of specific thermal resistances (due to the cold side and hot side convection, and heat exchanger metal surface conductivity) as in equation (5). Reference values for chevron-type heat exchangers overall heat transfer coefficients were provided by the heat exchanger manufacturer in the framework of the European project PUMPHEAT [39], based on butane (R600) working fluid and water as external heat transfer fluid, at cycle design conditions. Table 1 reports the specific thermal resistance values and the relative reference conditions. To account for different working fluids or operating conditions, the specific thermal resistance on the working fluid side is corrected according to equation (6), where φ_1 is the fluid correction factor, and φ_2 is the temperature and pressure correction factor. In equation (6) star-marked values are the specific thermal resistance computed on a chevron channel, for single-phase heat exchange [40], and on a flat plate for two-phase exchanges [41]. The subscript "ref" indicates the reference specific thermal resistance design value and the relative operating conditions provided by the manufacturer and reported in Table 1.

$$U = \frac{1}{k_{hot} + k_w + k_{cold}} \tag{5}$$

$$k = k_{ref} \cdot \varphi_1 \cdot \varphi_2 = k_{ref} \cdot \frac{k^*_{wf\ T_{ref} p_{ref}}}{k^*_{R600\ T_{ref} p_{ref}}} \cdot \frac{k^*_{wf\ T_x p_x}}{k^*_{wf\ T_{ref} p_{ref}}} = k_{ref} \cdot \frac{k^*_{wf\ T_x p_x}}{k^*_{R600\ T_{ref} p_{ref}}} \tag{6}$$

Pressure drop in all heat exchangers was assumed 5% of the inlet absolute pressure. For waste heat recovery purposes, all heat exchangers are imposed to be chevron-type plate heat exchangers.

Table 1: reference heat transfer coefficients, specific thermal resistances, and related operating conditions – reference values have been provided for R600.

	U_{ref} [W/m²K]	**$k_{cold\ ref}^{-1}$ [W/m²K]**	**$k_{w\ ref}^{-1}$ [W/m²K]**	**$k_{hot\ ref}^{-1}$ [W/m²K]**	**p_{ref} [bara]**	**T_{ref} [°C]**	**ΔT_{ref} [K]**
Evaporator	2340	2900	30000	19300	7.4		4
Evaporator bis	840	900			7.4	65	
Condenser	1410	19300		1600	21.8		15
Subcooler	2000			2400	21.7	107	
Desuperheater	1340			1500	21.8	132	
Regenerative superheater hot side	640	900		2400	21.6	84	
Regenerative superheater hot side					7.2	78	

Cost functions of heat exchangers, compressor, and motor are reported by Ommen et al. [33], then the cost accounts for the operating pressure by means of the correlation proposed by Seider [42], and finally have been adjusted for inflation to 2021 value basing on the European Central Bank Harmonized Indices of Consumer Prices [43].

2.2. Validation

The model is then validated using the Euroheat large HPs in DHN applications open database [44], already analyzed in detail in [45]. The database includes data from 102 HPs, but only for 54 of them sufficient information (capacity, supply temperature, source temperature, source type[1], working fluid, and COP) are provided for comparison against the model results. Figure 2 summarizes the performance of 55 HPs included in the validation process. The supply temperature of 34 of them is within the 3rd Generation District Heating Network, 3G DHN, Temperature Range (75-100°C), while the remaining 21, produce at the temperature level of a 4th Generation District Heating Network, 4G DHN. 38 of them adopt R717, 16 adopt R717, the remaining one R245fa.

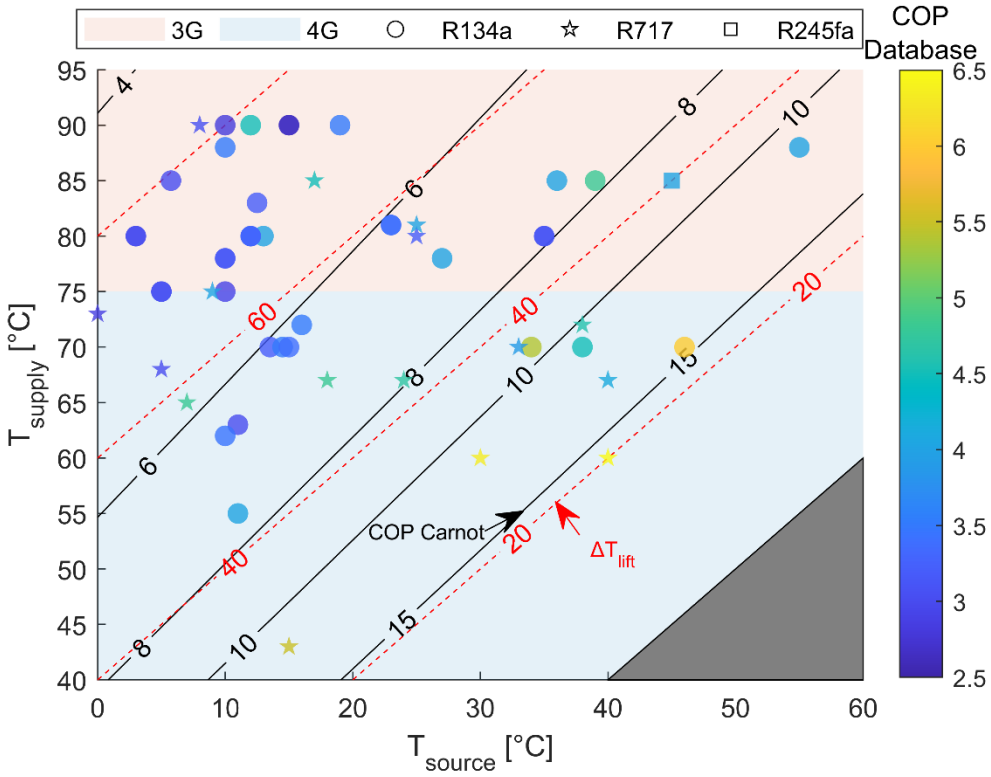

Figure 2: Euroheat HP dataset COP as a function of source and supply temperatures (red dashed line - temperature lift; black solid line - COP_{Carnot}).

$$\mathrm{COP}_{Carnot} = \frac{T_{supply}\ [\mathrm{K}]}{T_{supply}\ [\mathrm{K}] - T_{source}[\mathrm{K}]} = \frac{T_{supply}}{\Delta \mathrm{T}_{lift}} \tag{7}$$

In order to validate the HP model, it was fitted to the dataset by selecting a pinch point temperature difference (equal for all HXs) which minimizes the mean least squared of COP. $\Delta T_{HX\ pp\ min}$ was then considered equal for all the heat exchangers, while the ΔT_{SH} is chosen to maximize the ΔNPV, introduced within the following section, while χ is imposed at 100% (no IHX is considered). The procedure for selecting the ΔT_{SH} highlights that the optimal value, used for the purpose of validation, converges, for all the 55 HPs included in the dataset, to the lower bound of 5K. It confirms the finding

[1] According to the source type different evaporators are selected. Waste heat implies chevron plates, while water source HP are supposed to adopt shell-and-tubes evaporators. Also ΔT_{source} depends on the source type, 20K and 10K are imposed in the two cases respectively.

of [46], pointing out that, even if increased ΔT_{SH} may be beneficial on the COP, it implies an oversizing of the compressor and thus too high TCI increment.

$$\min_{\Delta T_{HX\ pp\ min}} \sum_{i=1}^{55} COP_{error_i}^{\ 2} \tag{8}$$

$$COP_{error_i} = COP_{Database_i} - COP_{model_i} \tag{9}$$

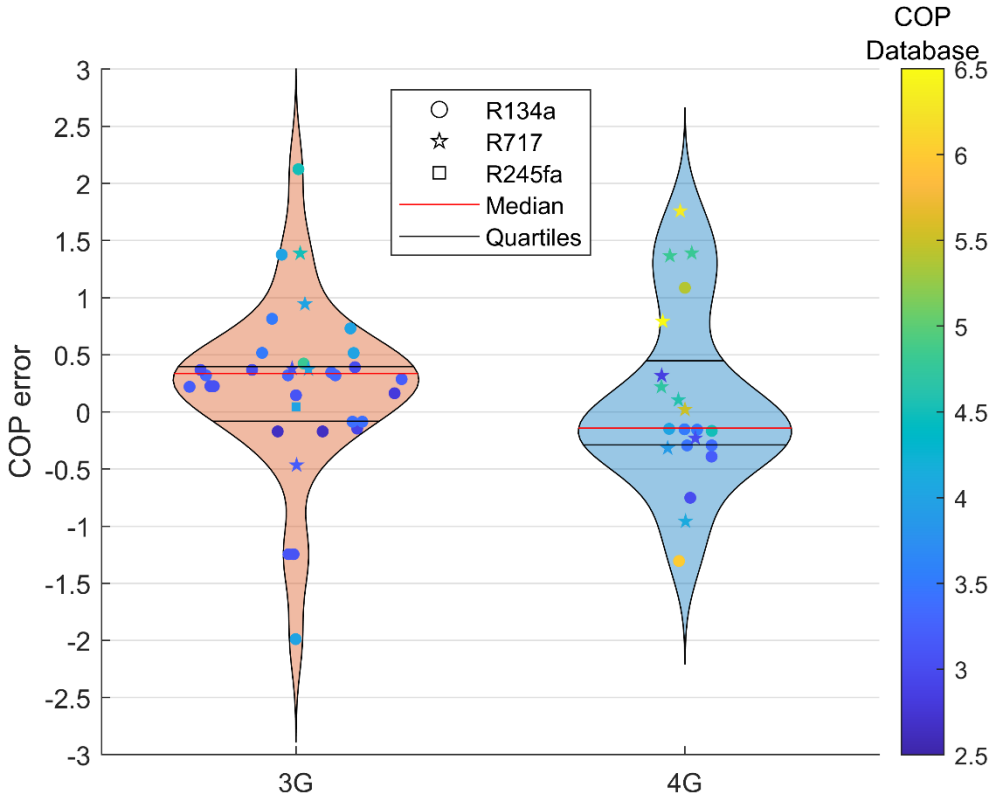

Figure 3: COP error distribution divided for HP supply temperature typical of 3G and 4G DHN, respectively

Figure 3 reports the validation error distributions for HPs whose thermal level is potentially such to feed 3G or 4G DHNs. For 71% of the data, the model absolute error is less than 0.5 on COP, moreover, the error is equally distributed for working fluid and operating conditions. Considering the large number of unknown or uncertain features and variables not reported in the validation dataset (including but not limited to source abundance, return temperature, and compressor efficiency, cycle architecture), outliers can be justified by significant differences between real and assumed operating conditions. As a final result, this detailed model, though assuming the schematic layout of Figure 1 for all HPs in the database, can be considered reliable enough for the purpose of the analysis presented in this paper.

2.3. Key performance indicators

TCI and COP are the first immediate indicators, the former represents the capital cost while the latter is proportional to the variable cost for operating the HP. However, a further parameter must be defined to find the best trade-off between the cost and the thermodynamic optimization. In order to estimate the profitability, the difference in Net Present Value (ΔNPV) between the heat pump and an already existing natural gas-fired Heat Only Boiler, HOB, working in the same condition, is assessed. This approach allows easy evaluation of heat pumps as a low-carbon alternative to traditionally employed fossil fuel-based technologies. Moreover, since comparison is on the same thermal demand, revenues from the heat supply are the same, and in computing the difference, no assumption on the thermal unit prices is needed.

$$\Delta NPV = NPV_{HP} - NPV_{HOB} \tag{8}$$

$$NPV_j = -TCI_j + \sum_{k=1}^{n} \frac{Revenue_j - FC_j - O\&M_j}{\left(1 + i_{eff}\right)^k} = -TCI_j + \sum_{k=1}^{n} \frac{Revenue_j - VC_j}{\left(1 + i_{eff}\right)^k} \tag{9}$$

The TCI is assumed to be zero for the HOB since it is considered as already existing, while for the HP, it is returned as an output by the described techno-economic model. The Operating and Maintenance costs are composed of a fixed part, 1900 €/MWyr for the HOB and 2000 €/MWyr for the HP, and a variable component. Variable O&M are assumed 1 €/MWh for the HOB and computed as it follows for the HP [47].

$$O\&M_{var_{HP}} = 2.7509 + 7 \cdot 10^{-5}(Capacity[kW]) \ \ [€/\text{MWh}] \tag{10}$$

i_{eff} is the effective interest rate over the lifetime of the system, calculated as below, where i is the interest rate and i_L is the inflation rate, assumed to be equal to 7% and 2%, respectively. The lifespan perspective is 20 years (n in equation (7)).

$$i_{eff} = \frac{1 + i}{1 + i_L} - 1 \tag{11}$$

Finally, fuel costs (FC) [€], i.e., gas and electricity consumption, depend on the efficiency of the two systems. In the HOB case, the fuel cost also includes the price of CO_2 emission allowances, assumed at 60 €/ton according to EU-ETS data. The Sum of FC and O&M is defined as Variable Costs (VC).

$$FC_{HP} = \frac{\dot{Q}}{COP} \cdot C_{el} \cdot \text{OH} \tag{12}$$

$$FC_{HOB} = \frac{\dot{Q}}{\eta_{HOB}} \cdot \left(C_{gas} + e \cdot C_{CO_2}\right) \cdot \text{OH} \tag{13}$$

η_{HOB} estimation is based on a literature model taking into account also flue gas condensation as a function of the water temperature at the boiler inlet. In this paper, the return temperature is fixed at 70°C corresponding to η_{HOB}=85.8%. [48].

Finally, the Internal Rate of Return (IRR) is defined as the i_{eff} that would set the ΔNPV equal to zero.

3. Working Fluid Comparison Through Optimisation

The present section uses the introduced detailed model on the basis of WTEMP EVO to benchmark different fluids, to investigate how the source temperature and the supply temperature impact the optimal COP and TCI of heat pumps exploiting waste heat as a thermal source. Component assumptions, such as compressor efficiency, temperature differences, etc., are those resulting from the previous validation against the Euroheat database. CoolProp opensource library is used to compute the thermodynamic properties [49], and therefore the analysis is limited to the fluids included in the library (including also thermal conductivity and viscosity). Different low GWP fluids are benchmarked against the HFC standards R134a and R245fa. Investigated supply temperatures are in the range of 60-120°C (15K step), with source temperature from 30°C to 70°C (20K step), and 7 different HPs sizes are considered between 50kW_{th} and 5MW_{th}.

Figure 4 reports the Pareto fronts as a result of the multi-objective optimization, MOO, carried out through the paretosearch algorithm in MATLAB [50], upper and lower bounds to the optimization variables are set as inTable 2: Optimization variables upper and lower bounds. Visualization does not include the full set of investigated sizes, supply, and source temperatures but it is limited to 1MW_{th}, T_{supply} of 60°C, 90°C, typical of 4G and 3G DHN, and 120°C, typical of 2G DHN and low-temperature

industrial-process heat. Finally, two source temperatures are shown, 30°C, as the low-temperature recoverable potential described by [6,51], and 70°C.

Table 2: Optimization variables upper and lower bounds

Variable	Symbol	Lower bound	Upper Bound
Minimum Condenser pinch point temperature difference	$\Delta T_{COND\ pp\ min}$	5K	15K
Minimum Subcooler pinch point temperature difference	$\Delta T_{SC\ pp\ min}$	5K	15K
Minimum Evaporator pinch point temperature difference	$\Delta T_{EVA\ pp\ min}$	5K	15K
Minimum IHX pinch point temperature difference	$\Delta T_{IHX\ pp\ min}$	5K	15K
Superheating at the compressor suction	ΔT_{SH}	5K	40K
Fraction of superheating provided by the evaporator	χ	0%	100%

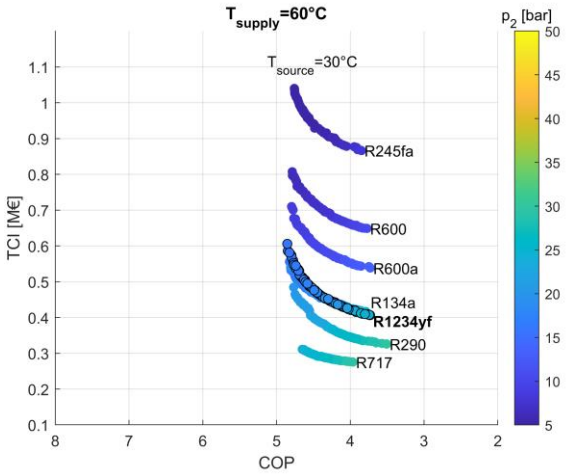

(a1)

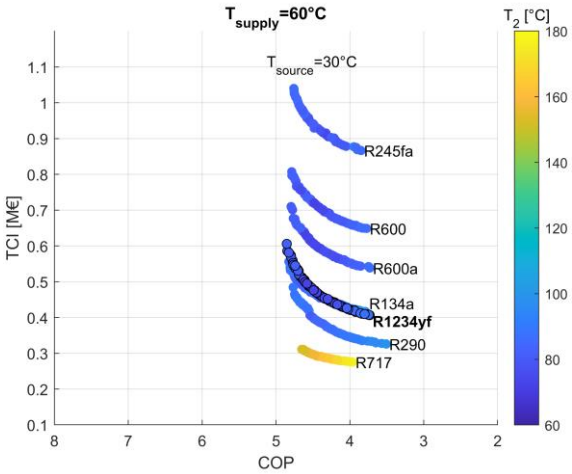

(a2)

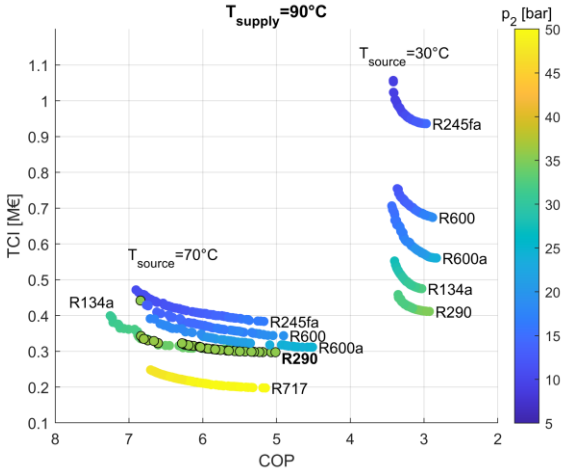

(b1)

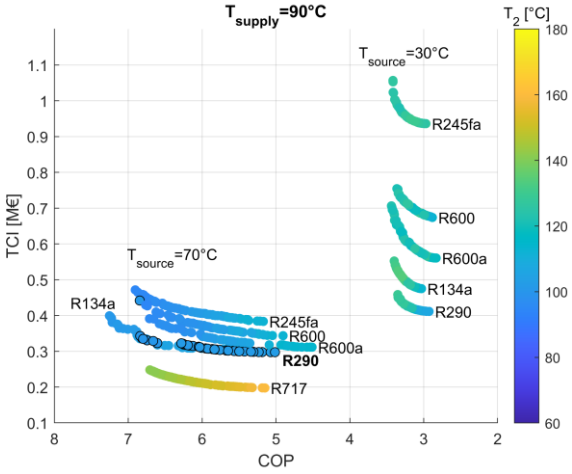

(b2)

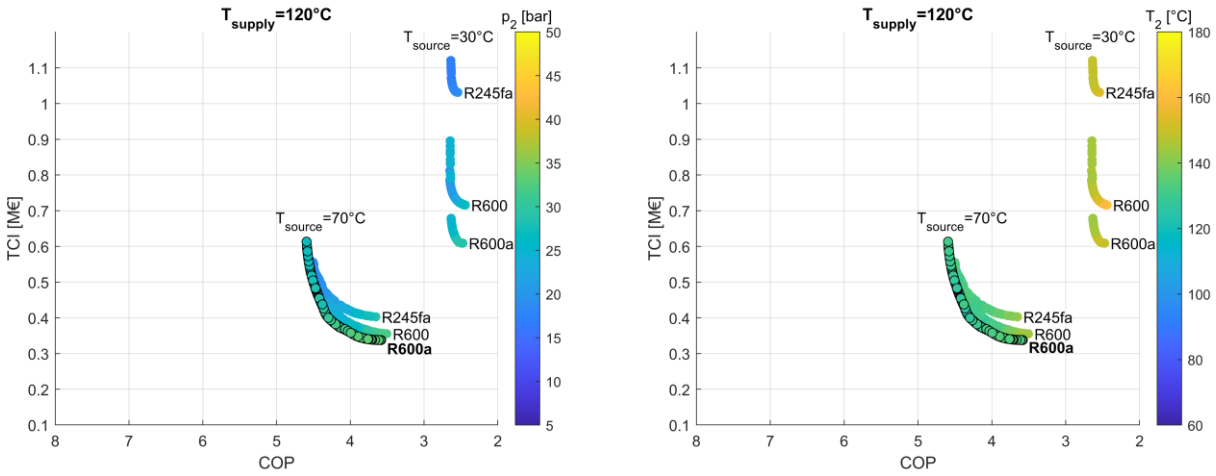

(c1) *(c2)*

Figure 4: 1MW$_{th}$ HP, TCI and COP multi-objective optimization Pareto fronts for (a) 4G DHN, (b) 3G DHN, and (c) 2G DHN; colors highlight (1) compressor discharge pressure and (2 temperature. Bold fluid names correspond to black-edged points.

Figure 4 highlights that the influence of fluid on the achievable COP is almost negligible, while similar operating temperatures play a major role, however, the working fluid significantly affects the TCI. Moreover, considering different sources and supply temperatures, the fluids economic merit is unchanged. R245fa implies the highest costs of investment, followed by butane (with the two considered isomers R600 and R600a) and R134a is almost equivalent to R1234yf. Finally, propane (R290) and especially ammonia (R717) are the fluids requiring the cheapest equipment. However, not all the fluids are suitable for the considered applications, considering the cycle architecture as in Figure 1, with a single-stage reciprocating compressor. In the cases where discharge temperature and pressure exceed the limit values (180°C and 50 bar), or supply temperature is not achievable through a subcritical cycle because of the low critical temperature, fluids are not plotted in Figure 4.

The following equations indicate the highest achievable temperatures of supply for each fluid. R717 supply temperature is limited by the maximum pressure and temperature at the compressor discharge, since the HP design strongly impacts the discharge conditions the maximum achievable supply depends on whether a COP maximization or a TCI reduction is pursued. Equations (16) and (17) indicate the respective limits as a function of T_{source}. For intermediate designs, the actual limit can be interpolated between these two values. Concerning the other fluids, the maximum supply temperature is imposed by the constraint of limiting the condensing pressure to the critical value. Considering a non-constant sink temperature, the maximum supply temperature complying with the limit of subcritical condensing pressure differs from the critical temperature by a value δ_{crit}. Such a value depends on several factors including, but not limited to, the source temperature, the superheating at the compressor suction, the χ factor, and specific heat at constant pressure of fluid superheated vapor. Considering all these factors the following equations quantify δ_{crit} for each fluid under the assumptions of this paper; since the dependency on T_{source} and COP is limited, in the following the average value is reported. Equations (18-23) report the theoretical limits beyond which it is practically impossible to supply heat through a subcritical cycle.

$$T_{supply\,max_{R717\,COP_{max}}} = \begin{cases} 44.6 + 0.9928 \cdot T_{source}, & T_{source} < 51.20°C \\ 104.20 - 0.1593 \cdot T_{source}, & T_{source} \geq 51.20°C \end{cases} \quad (16)$$

$$T_{supply\,max_{R717\,TCI_{min}}} = \begin{cases} 28.50 + 0.859 \cdot T_{source}, & T_{source} < 60.35°C \\ 87.26 - 0.1102 \cdot T_{source}, & T_{source} \geq 60.35°C \end{cases} \quad (17)$$

$$T_{supply\,max_{R290}} = T_{crit\,R290} + \delta_{crit\,R290} \approx 96.74 + 3.0 \approx 99.7 \quad (18)$$

$$T_{supply\,max_{R1234yf}} = T_{crit_{R1234yf}} + \delta_{crit\,R1234yf} \approx 94.70 + 0.6 \approx 95.3 \quad (19)$$

$$T_{supply\,max_{R134a}} = T_{crit_{R134a}} + \delta_{crit\,R134a} \approx 101.06 + 0.6 \approx 101.7 \quad (20)$$

$$T_{supply\,max_{R600a}} = T_{crit_{R600a}} + \delta_{crit\,R600a} \approx 134.67 + 2.6 \approx 137.3 \quad (21)$$

$$T_{supply\,max_{R600}} = T_{crit_{R600}} + \delta_{crit\,R600} \approx 151.98 + 2.9 \approx 154.9 \quad (22)$$

$$T_{supply\,max_{R245fa}} = T_{crit_{R245fa}} + \delta_{crit\,R245fa} \approx 153.86 + 0.9 \approx 154.8 \quad (23)$$

Generalizing the results and matching the merit order, out of Figure 4, with the limit to the maximum supply temperature, expressed by equations (16-23), it is possible to identify the best fluid for any combination of T_{source} and T_{supply}, as in Figure 5. Regardless of its toxicity, ammonia is today the best alternative for low and medium-temperature HPs. Nevertheless, high supply temperatures lead to extremely high condensing pressures, limiting the applicability. Moreover, low source temperatures imply very high temperatures at the end of the compression, and ΔT_{lift} greater than 44K cannot be adopted. Within this simulation, a lower bound on ΔT_{SH} is imposed equal to 5K. Pursuing a COP maximization (Figure 5a), rather than a TCI minimization (Figure 5b), condensing pressure is lower, therefore it is possible to extend the R717 operative range: however, considering 50 bar and 180°C as compressor discharge limits, it is not possible to supply heat beyond 96°C, this maximum value is achieved for a source of 51C°.

For increased supply temperatures Propane (R290), Iso-Butane (R600a), and N-Butane (R600) are selected as the best fluids for intermediate, high, and extremely high temperatures, respectively. These fluids are not limited by discharge conditions since the respective critical points do not exceed 50 bar nor 180°C. Nevertheless, the critical temperature limits the achievable T_{supply} by means of subcritical thermodynamic cycles. Limits are shown in Figure 5 according to the δ_{crit} value expressed by equations (18-23).

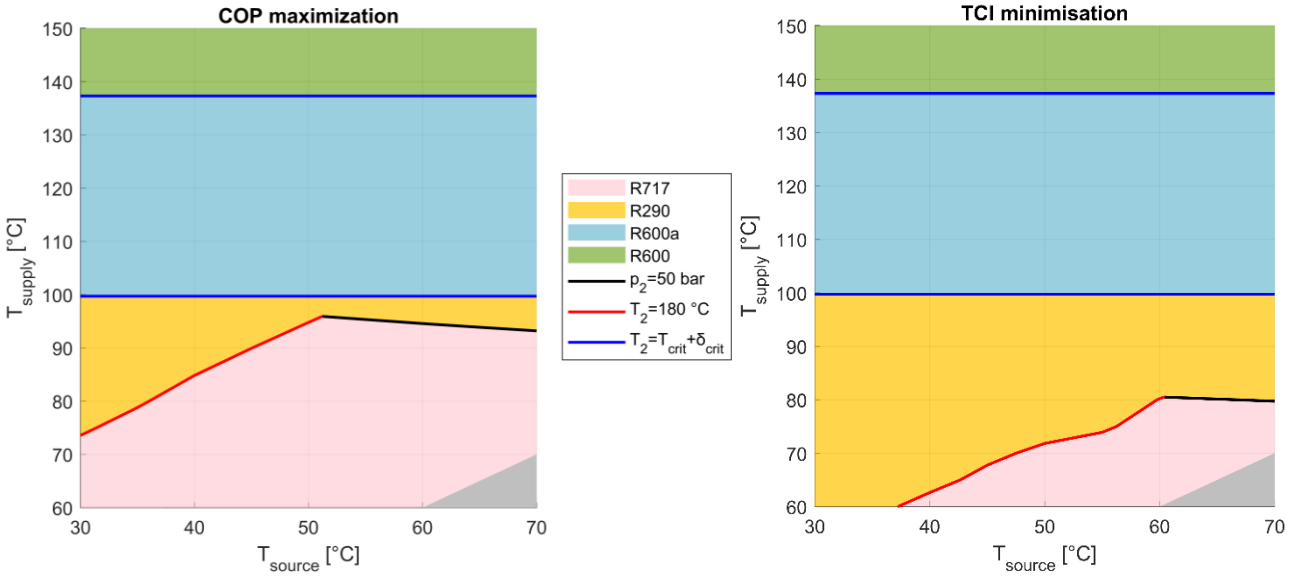

(a) *(b)*

Figure 5: Temperature domain of best fluid obtained by matching the economic merit order from Figure 6 and the supply limit as in equations (16-23) under the two extreme optimization conditions (a)COP maximization, (b) TCI minimization

4. Advanced Cost functions definition

From the multi-objective optimization results performed with the detailed WTEMP EVO-based model validated on the Euroheat database, it is possible to develop dedicated cost functions for HPs employing specific working fluids. The mathematical formulation of such new cost functions is based on the assumption that, as it can be demonstrated, the shape of Pareto fronts does not depend on HP capacity and can be fitted by a power function that summarize the relation between the COP and TCI. Such function quantifies the Performance Factor (*PF*) i.e. the impact on TCI of COP variation with respect to the baseline.

The equation (24) highlights the contribution of the three major design factors on the TCI: the operating conditions, $\overline{TCI}_{1000}$ (i.e., the average TCI for a 1000 kW_{th} HP), the selected COP, *PF*, the HP size, summarized by the scaling parameter α. Equation (25), *PF*, fits the dimensionless Pareto front (i.e., the Pareto set divided by the average TCI and COP) of a 1000 kW_{th} HP and it can be evaluated in the range of $COP_{TCImin}<COP<COP_{COPmax}$ to adjust the HP design in the direction of efficiency maximization or installation cost reduction. For a simplified calculation, the factor *PF* can be considered equal to 1.

COP_{TCImin} and COP_{COPmax} are the COP corresponding to the minimum TCI Pareto front's point and the best thermodynamically achievable COP (keeping constant the component performance assumptions, as discussed in the validation section). For a given source and supply temperature, they can be evaluated through equations (26) and (27) assessing the gap with the ideal COP_{Carnot}, equation (8), in order to quantify real operation losses. Finally, $\overline{TCI}_{1000}$ and $\overline{COP}_{1000}$ (the average COP for 1000 kW_{th} HP) are fitted by correlations (28) and (29).

$$TCI = TCI_{1000} \cdot \left(\frac{X\,[kW_{th}]}{1000}\right)^{\alpha} = \overline{TCI}_{1000} \cdot PF \cdot \left(\frac{X\,[kW_{th}]}{1000}\right)^{\alpha} [€] \tag{24}$$

$$PF = \frac{TCI_{1000}}{\overline{TCI}_{1000}} = A\left(\frac{COP}{\overline{COP}_{1000}}\right)^{B} + C\ [-] \tag{25}$$

$$COP_{TCImin} = \left(a \cdot T_{supply} + b \cdot \Delta T_{lift} + c\right) \cdot COP_{carnot}\ [-] \tag{26}$$

$$COP_{COPmax} = \left(d \cdot T_{supply} + e \cdot \Delta T_{lift} + f\right) \cdot COP_{carnot}\ [-] \tag{27}$$

$$\overline{TCI}_{1000} = D + E \cdot \Delta T_{lift} + F \cdot T_{supply}\ [€] \tag{28}$$

$$\overline{COP}_{1000} = G + H \cdot \Delta T_{lift} + I \cdot T_{supply} + J \cdot \Delta T_{lift}^{\,2} + K \cdot \Delta T_{lift} \cdot T_{supply}\ [-] \tag{29}$$

The first step is to fit $\overline{TCI}_{1000}$ and the dimensionless Pareto front. As explained in the previous section, the multiple objective optimization was performed for different combinations of T_{supply} and ΔT_{lift}, so that for each fluid we have between 6 and 21 couples of values as many Pareto sets, according to the feasibility constraints imposed by the fluid. The average values of each Pareto set are fitted as in eq.(28-29) against the supply temperature and lift. The $\overline{TCI}_{1000}$ fitting procedure report an average adjusted R^2 of 0.9031 with a maximum of 0.9641 for R134a and a minimum of 0.7792 for R290, concerning $\overline{COP}_{1000}$ the average adjusted R^2 is 0.9588 varying between 0.8680 and 0.9935 limits, corresponding to R717 and R245fa respectively.

Subsequently, the parameters A, B, and C (eq.25) are determined by seeking the best fit of all available dimensionless Pareto sets. Fitting results are shown in the figure, reporting on the chart the adjusted R^2 value.

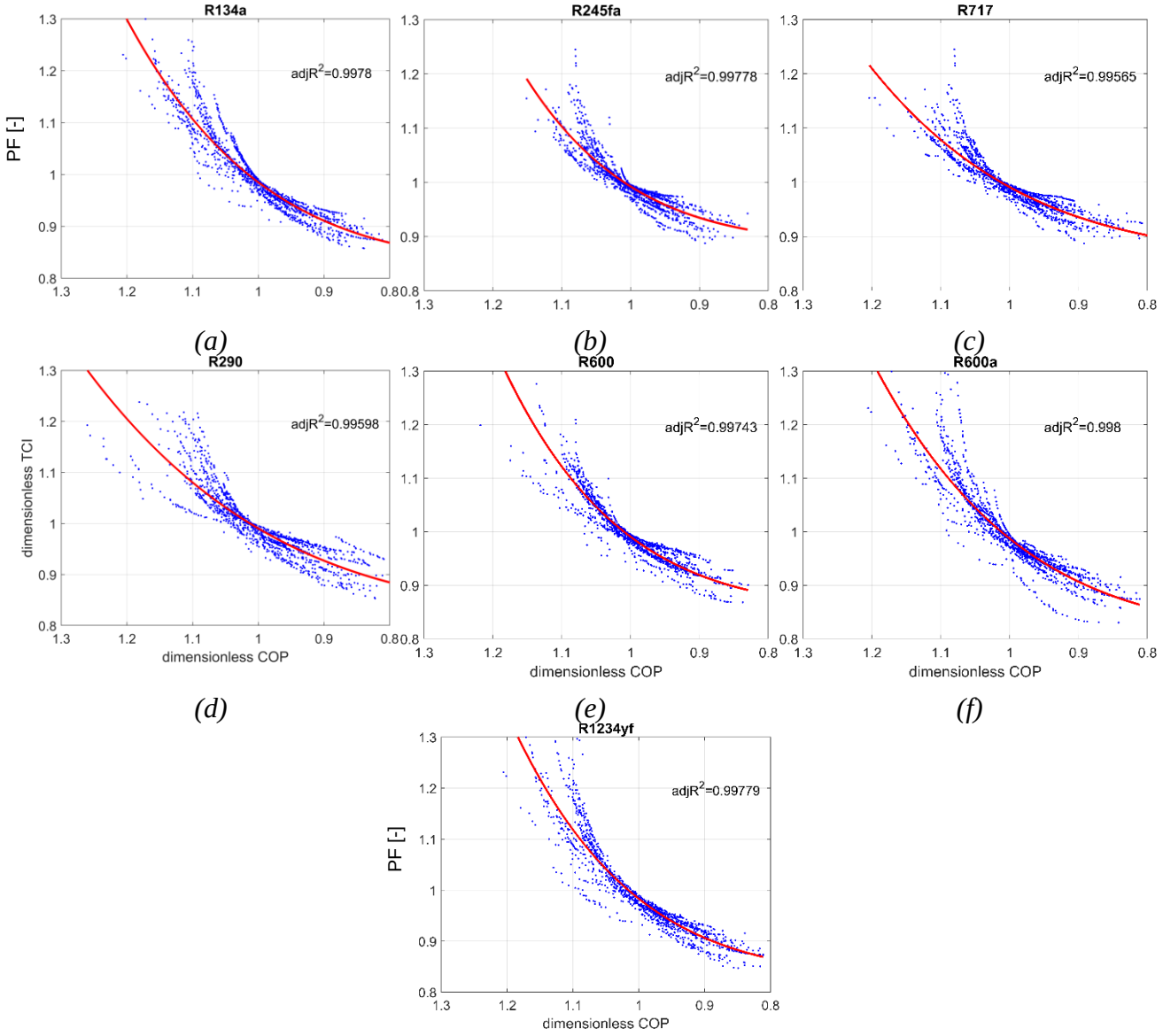

Figure 6: Power fitting of dimensionless Pareto fronts for 1MW$_{th}$ HP

Finally, the last fitting accounts for the impact of size on the cost. For each point of all available Pareto sets, TCI_{1000} is computed by means of the fitted equations (24-28). This term represents the expected TCI for a 1000 kW_{th} HP, it takes into account the impact of T_{supply}, ΔT_{lift}, and COP on the cost of investment. Then the actual TCI (i.e., the output of the full-detailed techno-economic model described in section 2) is fitted against TCI_{1000} and the HP size. The results of the fitting procedure are shown in Figure 7.

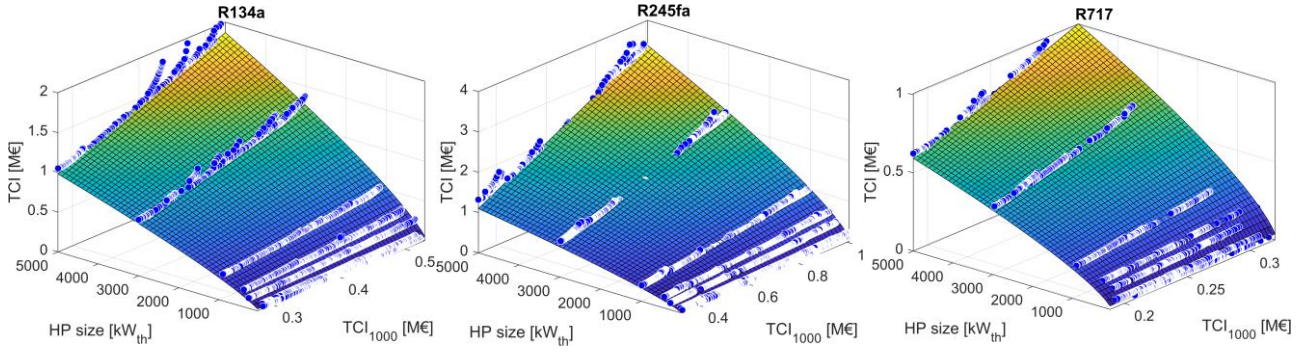

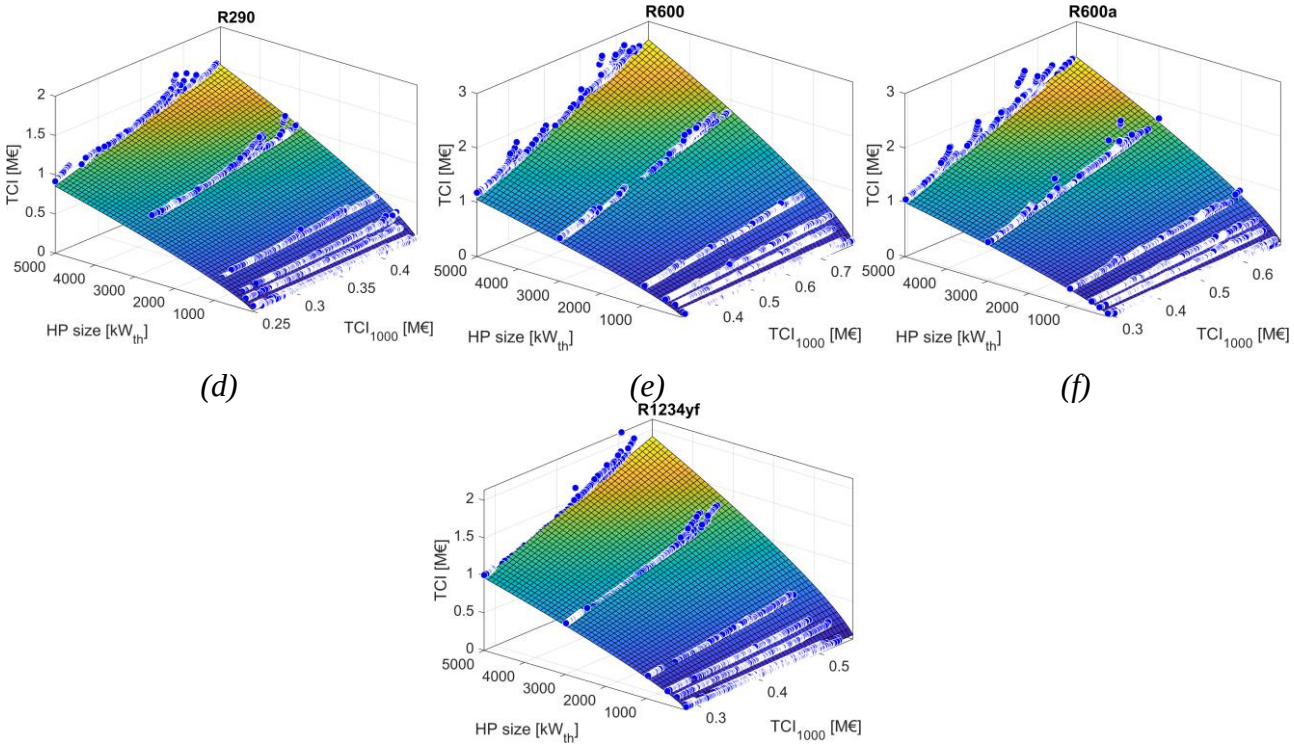

Figure 7: TCI fitting against TCI_{1000} and HP size for different fluids: (a) R134a, (b)R245fa, (c)R717, (d)R290, (e)R600, (f)R600a, (g)R1234yf

Coefficients for equations (16-21) are provided for each fluid in Table 3 and Table 4. Moreover, both adjusted R^2 and the Root Mean Squared Error (RMSE) are reported as regression goodness indicators of the final fitting (eq.(16)) to the model results.

Table 3: cost function parameters

	R134a	**R245fa**	**R717**	**R290**	**R600**	**R600a**	**R1234yf**
α [-]	0.78443	0.75195	0.71299	0.76557	0.75529	0.76098	0.7663
A [-]	0.1613	0.1052	0.12505	0.16553	0.13519	0.17509	0.15119
B [-]	5.8614	7.5387	5.5427	4.563	7.1156	5.8301	6.7072
C [-]	0.82499	0.88701	0.86589	0.82471	0.85521	0.81192	0.83181
D [€]	$1.3223\cdot10^{6}$	$4.8744\cdot10^{6}$	$7.7689\cdot10^{5}$	$5.4505\cdot10^{5}$	$3.1567\cdot10^{6}$	$2.2529\cdot10^{6}$	$1.7255\cdot10^{6}$
E [€/K]	4658.1	14340	2437.5	3247.2	8619.7	6282.9	4846.7
F [€/K]	-3034.3	-13224	-1700.1	-866.83	-8195.7	-5610.6	-4223
G [-]	-3.0202	0.7241	-2.713	-7.883	2.1923	3.0708	-14.519
H [K^{-1}]	-0.094519	-0.076573	-0.12191	0.10353	-0.089934	-0.13482	0.45482
I [K^{-1}]	0.03198	0.019635	0.033355	0.043282	0.014873	0.012003	0.06528
J [K^{-2}]	$8.6747\cdot10^{-4}$	$5.5891\cdot10^{-4}$	$2.7393\cdot10^{-3}$	$6.5222\cdot10^{-4}$	$5.4214\cdot10^{-4}$	$4.3302\cdot10^{-4}$	$1.2373\cdot10^{-3}$
K [K^{-2}]	$-1.2753\cdot10^{-4}$	$-9.648\cdot10^{-5}$	$-2.8766\cdot10^{-4}$	$-6.0665\cdot10^{-4}$	$-4.7105\cdot10^{-5}$	$9.8711\cdot10^{-5}$	$-1.7599\cdot10^{-3}$
R^2 [-]	0.99701	0.99168	0.99739	0.99232	0.99531	0.99465	0.99542
RMSE [M€]	0.027326	0.076311	0.013166	0.036573	0.044750	0.041967	0.033241

Table 4: COP domain fitting coefficient

		R134a	**R245fa**	**R717**	**R290**	**R600**	**R600a**	**R1234yf**
COP_{TCI}	**a [-]**	$1.1973\cdot10^{-3}$	$1.4603\cdot10^{-4}$	$1.1231\cdot10^{-3}$	$6.2798\cdot10^{-6}$	$-1.5086\cdot10^{-4}$	$-1.6648\cdot10^{-4}$	$-2.0761\cdot10^{-6}$
	b [K^{-1}]	$6.9318\cdot10^{-3}$	$5.6128\cdot10^{-3}$	$9.8569\cdot10^{-3}$	$6.8603\cdot10^{-3}$	$5.572\cdot10^{-3}$	$5.7728\cdot10^{-3}$	$7.4746\cdot10^{-3}$
	c [K^{-1}]	-0.29168	0.1152	-0.32175	0.10431	0.21209	0.2037	0.10226
	R^2 [-]	0.83806	0.89071	0.73035	0.77763	0.89958	0.87746	0.94443

	RMSE [-]	0.27731	0.24779	0.27372	0.27614	0.23141	0.23374	0.12692
COP_{COPmax}	**d [-]**	$8.5988 \cdot 10^{-4}$	$5.4569 \cdot 10^{-4}$	$7.4129 \cdot 10^{-4}$	$7.0592 \cdot 10^{-4}$	$3.0832 \cdot 10^{-4}$	$3.7712 \cdot 10^{-4}$	$-1.8086 \cdot 10^{-4}$
	e [K^{-1}]	$6.2681 \cdot 10^{-3}$	$5.0873 \cdot 10^{-3}$	$9.2692 \cdot 10^{-3}$	$6.4875 \cdot 10^{-3}$	$5.1431 \cdot 10^{-3}$	$5.1276 \cdot 10^{-3}$	$7.5503 \cdot 10^{-3}$
	f [K^{-1}]	-0.057935	0.071051	-0.083023	-0.015112	0.15258	0.12734	0.26135
	R^2 [-]	0.94042	0.92081	0.92804	0.93342	0.93352	0.9341	0.96734
	RMSE [-]	0.30059	0.33627	0.22192	0.30455	0.30798	0.3041	0.18791

While in general the parameters of equations (24-29) cannot be compared per se, the scale factor α retains its meaning of specific capital cost reduction with the installed capacity, since it is always lower than 1: for all fluids, it is in the range between 0.713 (R717, ammonia) that is the fluid most favored by a large capacity and 0.784 for R134a.

5. Case study: HOB replacement by HP through NPV optimization

This section provides an example of applications of the new cost functions, previously presented, for a twofold objective: demonstrating the engineering potential in estimating the best HP system for a specific application and verifying the cost function correlation accuracy against the original WTEMP-EVO-based detailed model.

Waste heat at 40°C is assumed as a thermal source and ΔT_{source}=20K is imposed. Three different cases are considered:

1. T_{supply}=115°C, adopting iso-butane (R600a) as working fluid
2. T_{supply}=95°C, adopting propane (R290) as working fluid
3. T_{supply}=80°C, adopting ammonia (R717) as working fluid

In such conditions both T_{source} and T_{supply} are different from the values at which the techno-economic model was run to fit the new advanced cost functions. For the purpose of this section, under these three circumstances, the profitability of replacing an existing natural gas-fired heat-only-boiler with an HP for $3MW_{th}$ size and 3000 annual operating hours is assessed. IRR and ΔNPV are assumed as a profitability indicator, gas and electricity price are considered as the average of EU27 during the period 2017-2021, consistently with [46].

First, the HP design is optimized by means of the WTEMP EVO-based techno-economic model to maximize ΔNPV, seeking the best trade-off between the COP maximization and TCI reduction – results in column (i) of Table 4. Second, the optimal COP is used as input for the new cost functions, presented in Section 4, comparing the results against the detailed techno-economic model on TCI and ΔNPV estimations. The percentage error on the TCI estimation reported in bolted font – results in column (ii) of Table 4 – quantifies the deviation between cost functions and the techno-economic model for the same input conditions. Third, the proposed cost functions are used independently and the optimization algorithm searches for the best COP maximizing ΔNPV – results in column (iii) of Table 4.

Table 5: Advanced cost functions application for assessing the profitability of replacing a HOB for different temperatures of supply and working fluids.

	T_{source} [°C]	T_{supply} [°C]	Fluid		(i) Technoeconomic model optimization	(ii) Cost functions		(iii) Cost functions optimization	
					Value	Value	Error vs. (i)	Value	Error vs. (i)
1	40	80	R717	COP	4.486	4.486		4.852	+8.1%
				TCI [M€]	0.643	0.592	**-7.9%**	0.632	-1.7%
				IRR	50.02%	56.74%	+6.7 pp	58.96%	+8.94 pp
2		95	R290	COP	3.714	3.714		4.027	+8.4%
				TCI [M€]	0.972	0.996	**+2.5%**	1.095	+12.6%
				IRR	21.98%	21.28	-0.70 pp	22.25	-0.23 pp
3		115	R600a	COP	3.250	3.250		3.453	+6.2%
				TCI [M€]	1.332	1.336	**+2.6%**	1.514	+13.4%
				IRR	10.07%	9.64%	-0.43 pp	10.2%	+0.13 pp

As it is possible to appreciate in Table 5, the use of the newly developed cost functions – column (ii) – implies quite small deviations from the full detailed techno-economic assessment, considering the same COP of (i) (grey color in column (ii) indicate that COP is an input for the cost correlations): percentage errors on TCI of -7.9%, +2.5%, and +0.3% are reported for cases 1, 2, and 3 respectively. Considering the IRR, the error increase for case 1 up to 6.7 but on an extremely high value not affecting the assessment of invesment.

The last column of Table 5 (iii), uses the newly developed cost functions to perform ΔNPV optimization. In this case, COP is also estimated based on previously defined correlations. The error on both TCI and IRR may be greater than in (ii) because the optimum COP found is different since it is optimized on the provided cost functions rather than on the techno-economic model. However, it can be concluded that the level of uncertainty introduced by the new cost functions is low, and thus these highly reliable for preliminary viability analysis of investing in HOB substitution.

6. Conclusions

This paper investigates the techno-economic performance of large-size vapor compression HPs, exploring the influence of working fluid and COP on capital cost. The analysis focuses on natural fluids and HFOs, characterized by low GWP, included in the open source library CoolProp, comparing them against two HFCs standards, i.e, R134a for low and medium-temperature HPs and R245fa for HTHPs.

For different source and supply temperatures, the best fluids are identified. R717 (ammonia) was found to be the best option for low temperatures, showing also the best scale economy with respect to the capacity, but its applicability is limited by the relevant operating temperatures and pressures. On the other hand, R290 shows an interesting potential for intermediate ranges (up to 100-110°C), and R600a, isobutane, is the best option for high-temperature HPs since it requires the cheapest equipment among the considered fluids.

From the presented Pareto analysis, detailed cost functions are provided accounting for the working fluid and the source and supply temperatures. COP value, within the feasibility range provided for each fluid and operating temperature, is a cost function input in order to consider the marginal cost of an efficiency increment. Furthermore, a simplified version of such cost functions is

also discussed, to allow for assessing an average expected cost for an HP characterized by an average COP.

These new cost functions address a gap in knowledge about the HP capital expenditure dependency on fluid, supply, and source temperature. Such cost functions can be applied to future techno-economic analyses keeping into consideration that (i) water was assumed as heat transfer fluid both on evaporator and condenser, (ii) the heat transfer fluid temperature difference ΔT_{source} is assumed 20K constant, and (iii) heat transfer fluid temperature difference ΔT_{supply} is a linear function of T_{supply}.

Finally, the paper presents three case studies comparing the proposed cost functions with the detailed techno-economic model. The three cases address the replacement of a natural gas-fired heat-only-boiler with an HP, identifying the best working fluid based on the different supply temperatures, as presented in Section 5. The TCI deviation between the detailed techno-economic analysis and the cost function analysis is limited to 7.9%, improving the goodness of the proposed cost functions for a first fast estimation of the heat pumps TCI in specific applications.

Glossary

Acronyms

CFC	Clorofluorocarbons
COND	Condenser
COP	Coefficient of Performance
DHN	District Heating Network
EVA	Evaporator
GWP	Global Warming Potential
HCFC	Hydroclorofluorocarbons
HFC	Hydrofluorocarbons
HFO	Hydrofluoroolefins
HCFO	Hydrochlorofluoroolefins
HP	Heat Pump
HTHP	High-Temperature Heat Pump
IHX	Internal Heat Exchanger
IRR	Internal Rate of Return
O&M	Operating and Maintenance cost
ODP	Ozone Depletion Potential
PEC	Purchasment Equipment Cost
PM	Particular Matter
pp	percentage points
RMSE	Root Mean Squared Error
SC	Subcooler
TFA	Trifluoracetic Acid
TRL	Technology Readiness Level
UN	United Nation

VC	Variable Cost
VHC	Volumetric Heat Capacity

Symbols and variables

A	[m^2]	Area
A	[-]	TCI-COP linear factor
a	[-]	COP_{min} constant factor
B	[-]	TCI -COP scale factor
b	[K^{-1}]	COP_{min} linear factor
C	[€/kWh]	Cost
C	[-]	TCI-COP constant factor
c	[K^{-1}]	COP_{min} linear factor
$\overline{COP}_{1000}$	[-]	Average COP for 1000 kW_{th} HP
COP_{1000}	[-]	Expected COP for 1000 kW_{th} HP
D	[€]	$\overline{TCI}_{1000}$ constant factor
d	[-]	COP_{max} constant factor
E	[€/K]	$\overline{TCI}_{1000}$ linear factor
e	[K^{-1}]	COP_{max} linear factor
F	[€/K]	$\overline{TCI}_{1000}$ linear factor
f	[K^{-1}]	COP_{max} linear factor
G	[-]	$\overline{COP}_{1000}$ constant factor
H	[K^{-1}]	$\overline{COP}_{1000}$ linear factor
I	[K^{-1}]	$\overline{COP}_{1000}$ linear factor
i	[-]	interest rate
i_{eff}	[-]	effective rate
i_L	[-]	inflation rate
J	[K^{-2}]	$\overline{COP}_{1000}$ quadratic factor
K	[K^{-2}]	$\overline{COP}_{1000}$ interaction factor
k	[W/m^2K]	Specific thermal resistance
LMTD	[K]	Logarithmic mean temperature difference
OH	[h]	Operative Hours
PF	[-]	Performance Factor
$\dot{Q}$	[kW]	Heat Flux
T	[°C] or [K]	Temperature
TCI	[€]	Total Cost of investment
$\overline{TCI}_{1000}$	[€]	Average TCI for 1000 kW_{th} HP
TCI_{1000}	[€]	Expected TCI for 1000 kW_{th} HP

U	[W/m^{2}K]	Overall heat transfer coefficient
X	[kW_{th}]	Capacity input to HP's cost function
α	[-]	TCI scale factor
Δ		Difference
η	[-] or [%]	Efficiency
φ_2	[-]	Specific thermal resistance working fluid correction factor
φ_2	[-]	Specific thermal resistance temperature and pressure correction factor
χ	[%]	Fraction of superheating provided by the evaporator

subscripts

HX	Heat Exchanger
min	Minimum
pp	Pinch point
ref	Reference
SH	Superheating
var	Variable
w	Wall

Bibliography

[1] IEA. Heating. Paris: 2021.

[2] Liu X, Wu J, Jenkins N, Bagdanavicius A. Combined analysis of electricity and heat networks. Appl Energy 2016;162:1238–50. https://doi.org/https://doi.org/10.1016/j.apenergy.2015.01.102.

[3] Persson U, Möller B, Werner S. Heat Roadmap Europe: Identifying strategic heat synergy regions. Energy Policy 2014;74:663–81. https://doi.org/10.1016/j.enpol.2014.07.015.

[4] Lu H, Price L, Zhang Q. Capturing the invisible resource: Analysis of waste heat potential in Chinese industry. Appl Energy 2016;161:497–511. https://doi.org/https://doi.org/10.1016/j.apenergy.2015.10.060.

[5] Grisolia T, Vannoni A, Sorce A, Calabria M. Sustainable opportunities to recover power plants' waste heat: a benchmark of techno-economically optimized heat pumps. Congr. ATI 2022, Bari: 2022.

[6] Lygnerud K, Wheatcroft E, Wynn H. Contracts, business models and barriers to investing in low temperature district heating projects. Appl Sci 2019;9. https://doi.org/10.3390/app9153142.

[7] Liu C, Han W, Xue X. Experimental investigation of a high-temperature heat pump for industrial steam production. Appl Energy 2022;312:118719. https://doi.org/https://doi.org/10.1016/j.apenergy.2022.118719.

[8] Stewart M. 9 - Reciprocating compressors. In: Stewart M, editor. Surf. Prod. Oper., Boston: Gulf Professional Publishing; 2019, p. 655–778. https://doi.org/https://doi.org/10.1016/B978-0-12-809895-0.00009-0.

[9] Nekså P, Rekstad H, Zakeri GR, Schiefloe PA. CO2-heat pump water heater: characteristics,

system design and experimental results. Int J Refrig 1998;21:172–9. https://doi.org/https://doi.org/10.1016/S0140-7007(98)00017-6.

[10] UNFCCC. Doha Amendment to the Kyoto Protocol. Doha: 2012.

[11] Lund H. Heat Roadmap Europe : Large-Scale Electric Heat Pumps in District Heating Systems Heat Roadmap Europe : Large-Scale Electric Heat 2017. https://doi.org/10.3390/en10040578.

[12] Pearson A. High Pressure Ammonia Systems – New Opportunities High Pressure Ammonia Systems – New Opportunities. Refrig Air Cond 2010:1–7.

[13] Pavlovic RT, Nopmongcol U, Kimura Y, Allen DT. Ammonia emissions, concentrations and implications for particulate matter formation in Houston, TX. Atmos Environ 2006;40:538–51. https://doi.org/https://doi.org/10.1016/j.atmosenv.2006.04.071.

[14] EEAP. Environmental Effects and Interactions of and Climate Change Depletion, UV Radiation, Stratospheric Ozone. Nairobi: 2019.

[15] Pearson A. High temperature heat pumps with natural refrigerants. IEA Heat Pump Cent Newsl 2012;30:33 – 35.

[16] Bless F, Arpagaus C, Bertsch SS, Schiffmann J. Theoretical analysis of steam generation methods - Energy, CO2 emission, and cost analysis. Energy 2017;129:114–21. https://doi.org/10.1016/j.energy.2017.04.088.

[17] Mateu-Royo C, Sawalha S, Mota-Babiloni A, Navarro-Esbrí J. High temperature heat pump integration into district heating network. Energy Convers Manag 2020;210:112719. https://doi.org/https://doi.org/10.1016/j.enconman.2020.112719.

[18] Park K-J, Jung D. Performance of heat pumps charged with R170/R290 mixture. Appl Energy 2009;86:2598–603. https://doi.org/https://doi.org/10.1016/j.apenergy.2009.04.009.

[19] ASHRAE. ASHRAE Standard 34 2020.

[20] McLinden MO, Kazakov AF, Steven Brown J, Domanski PA. A thermodynamic analysis of refrigerants: Possibilities and tradeoffs for Low-GWP refrigerants. Int J Refrig 2014;38:80–92. https://doi.org/https://doi.org/10.1016/j.ijrefrig.2013.09.032.

[21] Behringer D, Heydel F, Gschrey B, Osterheld S, Schwarz W, Warncke K, et al. Persistent degradation products of halogenated refrigerants and blowing agents in the environment : type, environmental concentrations, and fate with particular regard to new halogenated substitutes with low global warming potential. 2021.

[22] Fleet D, Hanlon J, Osborne K, Vedrine M La, Ashford P. Study on environmental and health effects of HFO refrigerants. 2017.

[23] Molés F, Navarro-Esbrí J, Peris B, Mota-Babiloni A, Barragán-Cervera Á, Kontomaris K (Kostas). Low GWP alternatives to HFC-245fa in Organic Rankine Cycles for low temperature heat recovery: HCFO-1233zd-E and HFO-1336mzz-Z. Appl Therm Eng 2014;71:204–12. https://doi.org/https://doi.org/10.1016/j.applthermaleng.2014.06.055.

[24] Patten KO, Wuebbles DJ. Atmospheric lifetimes and Ozone Depletion Potentials of trans-1-chloro-3,3,3-trifluoropropylene and trans-1,2-dichloroethylene in a three-dimensional model. Atmos Chem Phys 2010;10:10867–74. https://doi.org/10.5194/acp-10-10867-2010.

[25] Arpagaus C, Bless F, Uhlmann M, Schiffmann J, Bertsch SS. High temperature heat pumps: Market overview, state of the art, research status, refrigerants, and application potentials. Energy 2018;152:985–1010. https://doi.org/10.1016/j.energy.2018.03.166.

[26] Zhang S, Wang H, Guo T. Experimental investigation of moderately high temperature water source heat pump with non-azeotropic refrigerant mixtures. Appl Energy 2010;87:1554–61.

https://doi.org/https://doi.org/10.1016/j.apenergy.2009.11.001.

[27] Nanxi L, Shi L, Lizhong H, Mingshan Z. Moderately high temperature water source heat-pumps using a near-azeotropic refrigerant mixture. Appl Energy 2005;80:435–47. https://doi.org/https://doi.org/10.1016/j.apenergy.2004.02.005.

[28] Tomassetti S, Nicola G Di, Kondou C. Triple point measurements for new low- global-warming-potential refrigerants: Hydro-fluoro-olefins, hydro-chloro-fluoro-olefins, and trifluoroiodomethane. Int J Refrig 2022;133:172–80. https://doi.org/https://doi.org/10.1016/j.ijrefrig.2021.10.008.

[29] Bamigbetan O, Eikevik TM, Nekså P, Bantle M. Review of vapour compression heat pumps for high temperature heating using natural working fluids. Int J Refrig 2017;80:197–211. https://doi.org/https://doi.org/10.1016/j.ijrefrig.2017.04.021.

[30] Barco-Burgos J, Bruno JC, Eicker U, Saldaña-Robles AL, Alcántar-Camarena V. Review on the integration of high-temperature heat pumps in district heating and cooling networks. Energy 2022;239:122378. https://doi.org/https://doi.org/10.1016/j.energy.2021.122378.

[31] Jiang J, Hu B, Wang RZ, Deng N, Cao F, Wang C-C. A review and perspective on industry high-temperature heat pumps. Renew Sustain Energy Rev 2022;161:112106. https://doi.org/https://doi.org/10.1016/j.rser.2022.112106.

[32] De'Rossi F, Mastrullo R, Mazzei P. Working fluids thermodynamic behavior for vapor compression cycles. Appl Energy 1991;38:163–80. https://doi.org/10.1016/0306-2619(91)90031-R.

[33] Ommen T, Kj J, Brix W, Reinholdt L, Elmegaard B. Technical and economic working domains of industrial heat pumps : Part 1 e Single stage vapour compression heat pumps. Int J Refrig 2015;5.

[34] Traverso A, Massardo AF, Cazzola W, Lagorio G. WIDGET-TEMP: A Novel Web-Based Approach for Thermoeconomic Analysis and Optimization of Conventional and Innovative Cycles 2004:623–31. https://doi.org/10.1115/GT2004-54115.

[35] Baglietto G, Maccarini S, Traverso A, Bruttini P. Techno-Economic Comparison of Supercritical CO2, Steam, and ORC Cycles for WHR Applications. J Eng Gas Turbines Power 2022. https://doi.org/10.1115/1.4055727.

[36] Bejan A, Tsatsaronis G, Moran M. Thermal Design and Optimization. John Wiley & Sons, Inc.; 1996.

[37] Vannoni A. Flexible Heat and Power Generation: Market Opportunities for Combined Cycle Gas Turbines and Heat Pumps. University of Genoa, 2022. https://doi.org/http://hdl.handle.net/11567/1083022.

[38] Lund H, Werner S, Wiltshire R, Svendsen S, Eric J, Hvelplund F, et al. 4th Generation District Heating (4GDH) Integrating smart thermal grids into future sustainable energy systems. Energy 2014;68:1–11. https://doi.org/10.1016/j.energy.2014.02.089.

[39] https://www.pumpheat.eu 2017.

[40] Martin H. A theoretical approach to predict the performance of chevron-type plate heat exchangers. Chem Eng Process Process Intensif 1996;35:301–10. https://doi.org/10.1016/0255-2701(95)04129-X.

[41] Çengel YA. Heat Transfer: A Practical Approach. Second. McGraw-Hill; 2003.

[42] Seider WD, Lewin DR, Seader JD, Widagdo S, Gani R, Ng KM. Product and Process Design Principles. vol. 7. Fourth. Wiley; 2016.

[43] Eurostat. Harmonised index of consumer prices (HICP) (t_prc hicp) 2022.

[44] David A, Mathiesen BV, Averfalk H, Werner S, Lund H. Heat Roadmap Europe: Large-scale electric heat pumps in district heating systems. Energies 2017;10:1–18. https://doi.org/10.3390/en10040578.

[45] Vannoni A, Sorce A, Traverso A, Massardo AF. Techno-Economic Analysis of Power-to-Heat Systems. E3S Web Conf 2021;03003. https://doi.org/https://doi.org/10.1051/e3sconf/202123803003.

[46] Vannoni A, Sorce A, Traverso A, Massardo AF. Techno-economic Optimization of High-Temperature Heat Pumps for Waste Heat Recovery. Submitt Draft to Appl Energy n.d.

[47] Danish Energy Agency. Technology Data for Energy Plants for Electricity and District heating generation (v.0009 -April 2020) 2016.

[48] Satyavada H, Baldi S. A novel modelling approach for condensing boilers based on hybrid dynamical systems. Machines 2016;4. https://doi.org/10.3390/machines4020010.

[49] Bell IH, Wronski J, Quoilin S, Lemort V. Pure and Pseudo-pure Fluid Thermophysical Property Evaluation and the Open-Source Thermophysical Property Library CoolProp 2014. https://doi.org/10.1021/ie4033999.

[50] Custódio AL, Madeira JFA, Vaz AIF, Vicente LN. Direct multisearch for multiobjective optimization. SIAM J Optim 2011;21:1109–40. https://doi.org/10.1137/10079731X.

[51] ReUseHeat. Handbook for increased recovery of urban excess heat. 2022.